Chinese Chemical Letters 36 (2025) 109691

Contents lists available at ScienceDirect

Chinese Chemical Letters

journal homepage: www.elsevier.com/locate/cclet

Facilitating the polysulfides conversion kinetics by porous LaOCl nanofibers towards long-cycling lithium-sulfur batteries

Tengfei Yang, Jingshuai Xiao, Xiao Sun, Yan Song*, Chaozheng He*

Institute of Environment and Energy Catalysis, Shaanxi Key Laboratory of Optoelectronic Functional Materials and Devices, School of Materials Science and Chemical Engineering, Xi'an Technological University, Xi'an 710021, China

ARTICLE INFO

Article history:
Received 9 January 2024
Revised 3 February 2024
Accepted 29 February 2024
Available online 1 March 2024

Keywords:
Lithium-sulfur batteries
Polysulfides
Shuttle effect
LaOCl nanofibers
High sulfur loading

ABSTRACT

Lithium-sulfur batteries are considered to be a new generation of high energy density batteries due to their non-toxicity, low cost and high theoretical specific capacity. However, the development of practical lithium-sulfur batteries is seriously impeded by the sluggish multi-electron redox reaction of sulfur species and obstinate shuttle effect of polysulfides. In this study, a porous lanthanum oxychloride (LaOCl) nanofiber is designed as adsorbent and electrocatalyst of polysulfides to regulate the redox kinetics and suppress shuttling of sulfur species. Benefiting from the porous architecture and luxuriant active site of LaOCl nanofibers, the meliorative polarization effect and sulfur expansion can be accomplished. The LaOCl/S electrode exhibits an initial discharge specific capacity of 1112.3 mAh/g at 0.1 C and maintains a superior cycling performance with a slight decay of 0.02% per cycle over 1000 cycles at 1.0 C. Furthermore, even under a high sulfur loading of 4.6 mg/cm^2, the S cathode with LaOCl nanofibers still retains a high reversible areal capacity of 4.2 mAh/cm^2 at 0.2 C and a stable cycling performance. Such a porous host expands the application of rare earth based catalysts in lithium-sulfur batteries and provides an alternative approach to facilitate the polysulfides conversion kinetics.

As renewable energy sources and electric vehicles are being developed, electrochemical energy storage technology is challenged by high specific capacity and fast charging and discharging rate [1,2]. Lithium-sulfur batteries, due to their high theoretical specific capacity (1675 mAh/g), environmental friendliness, low cost and abundant sulfur monomer content, are considered to be one of the most promising next generation energy storage systems [3,4]. However, monomeric sulfur as cathode material for lithium-sulfur batteries still has some problems: (1) S and discharge product Li_2S_2/Li_2S are electron/ion insulators, resulting in low active material usage and poor battery cycling [5]. (2) The large density difference between sulfur and lithium sulfide causes a volume change of approximately 80% during cycling, leading to collapse of the electrode structure and irreversible damage to the battery [6]. (3) The polysulfide intermediates during charging and discharging tend to dissolve in the electrolyte, which generates a shuttle effect and in turn reduces the cycle life and Coulomb efficiency of the battery [7,8].

Over the past few decades, researchers have optimized various aspects of lithium-sulfur batteries to overcome the above issues, including the design of sulfur cathodes and the protection of the lithium anode. However, the fundamental problem of lithium-sulfur batteries is the defect of polysulfide intermediates that directly relates to the performance of cathode and anode. The rational design of lithium-sulfur battery cathodes is the effective breakthrough to solve the existing problems of lithium-sulfur batteries. To date, a number of conductive materials have been reported as sulfur host materials to improve the electrochemical performance of the sulfur cathode and limit the dissolution of polysulfides. Carbon materials are considered ideal as sulfur host materials due to their excellent electrical conductivity, tunable pore structure and high specific surface area [9–11]. However, the weak van der Waals forces between polar polysulfides and non-polar carbon-based materials only partially suppress the shuttle effect, leading to a rapid decrease in long-cycle capacity. Therefore, the introduction of a polar compound into a sulfur-based cathode can effectively immobilize the polysulfide because of the strong interaction between the polar surface and the polysulfide. These polar materials (including metal carbides [12,13], oxides [14–16], sulfides [17–19], nitrides [20,21]) can suppress the shuttle effect and accelerate the redox reaction of polysulfides, thus improving the performance of the batteries. Nonetheless, the catalytic activity of aforementioned adsorbents is generally suboptimal, which reduces the catalytic ability of the functional materials for polysulfides and ultimately in-

* Corresponding authors.
E-mail addresses: songyan@xatu.edu.cn (Y. Song), hecz2019@xatu.edu.cn (C. He).

https://doi.org/10.1016/j.cclet.2024.109691
1001-8417/

hibits the transport of electrons and ions, resulting in poor rate performance.

Compared to other transition metal ions, rare earth ions have a unique 4f orbital and electron, a large ionic radius and a strong self-polarising ability, which have a significant impact on the electrochemical performance of electrode materials [22]. The advantages of rare earth ions in electrode materials include improved structural stability of the electrode material, prevention of side reactions at the interface between the electrode material and the electrolyte, and improved electron and ion transport capabilities. The introduction of rare earth based polar catalytic materials in lithium-sulfur batteries systems will be conducive to firmly immobilize polysulfides through chemisorption and promote efficient conversion of polysulfides, which can fundamentally solve the problem of the shuttle effect and sluggish multi-electron redox reaction of sulfur species [23–25]. The rare earth compounds currently introduced into the cathode of lithium-sulfur batteries are mainly rare earth oxides [26] and rare earth hydroxides [27]. The superiority of rare earth compounds in improving the performance of lithium-sulfur batteries has made the search for other types of rare earth compounds a focus of research. The chemical interactions between rare earth oxides and polysulfides have been confirm, which can improve cathode anchoring effect and boost conversion reaction for sulfide species. Significantly, introducing electronegative halogens into metal oxides can alter the three-dimensional oxygen 2p orbital hybridisation of metals, bringing the center of the O p band closer to the Fermi energy level and thus more strongly modulating the electronic structure of metal catalysts and significantly improving catalytic activity [28,29]. In addition, the rare earth oxychloride is a two-dimensional polar layered material that has been exploited primarily as a highly efficient photocatalyst [30–32]. The empty orbitals of rare earth readily provide polarity-rich active sites and accept outer electrons from polysulfides, which can be used to alleviate the dissolution of polysulfides based on the strong chemisorption and catalytic effect to polysulfides.

Motivated by the above research, porous LaOCl nanofibers as host materials were proposed and prepared for modifying sulfur cathode and catalyzing polysulfide conversion. The LaOCl nanofibers with porous structure and high specific surface area provide abundant active sites for adsorption and catalytic conversion of sulfide species. The comprehensive computational and experimental analysis robustly reveals effective chemical anchoring by sulfophilic and lithiophilic sites and catalyzing conversion reactions for polysulfides. By virtue of the above advantages, LaOCl/S electrode can improve the reversible capacity and redox reaction kinetics of lithium-sulfur batteries.

LaOCl nanofiber were synthesized by electrostatic spinning and double-crucible heating treatment [33,34]. The porous LaOCl nanofibers have a large specific surface area, providing more active sites for increased loading of active sulfur. The synthesis process is depicted in Fig. 1a. Fig. 1b and Fig. S1 (Supporting information) show the SEM images of the prepared LaOCl nanofibers, which maintain the continuous one-dimensional morphology with a rough surface of about 200 nm in diameter and exhibit a disordered interlaced fibrous network architecture. The consecutive and interlaced farmwork as sulfur host will accommodates the volume expansion during electrochemical reaction process. The transmission electron microscopy (TEM) image confirms a porous structure of LaOCl nanofibers (Fig. 1c), which actually expands sulfur loading space and catalytic active areas for sulfur species. In addition, the high-resolution transmission electron microscopy (HRTEM) image (Fig. 1d) shows a lattice fringe spacing of 0.35 nm, which matches the (101) plane of LaOCl. The EDS elemental mapping images of LaOCl nanofibers (Figs. 1e-h) reveal show the uniform distributions of La, O, and Cl elements.

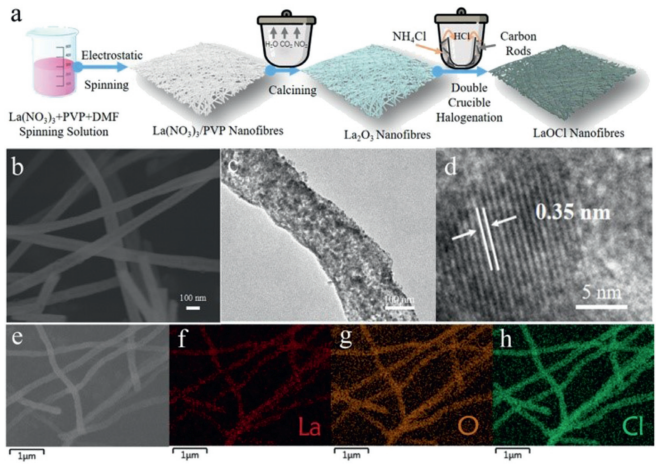

Fig. 1. (a) Schematic illustration for the synthesis of LaOCl nanofibers; (b) SEM image, (c) TEM image, (d) HRTEM image, and (e-h) EDS elemental mapping images of LaOCl nanofibers.

The X-ray diffraction pattern (Fig. S2 in Supporting information) of the prepared LaOCl nanofibers shows a good crystalline and are indexed to the standard card (JCPDS No. 88–0064). In principle, the high specific surface area can provide more adsorption active sites to enable the sufficient anchoring of polysulfides. Therefore, it is essential to study and analyse the specific surface area and pore distribution of the functional nanofibers using the Brunner-Emmett-Teller method. The N_2 adsorption-desorption isotherm of LaOCl (Fig. S3 in Supporting information) indicates a high specific surface area of 205.93 m^2/g and the presence of mesopores and micropores in the architecture. The rich porosity can endow LaOCl nanofibers with luxuriant active sites. The number of active sites has a direct impact on the cycling performance and multiplicative performance of the lithium-sulfur batteries, signifying that the prepared LaOCl nanofibers will enhance the utilisation of active sulfur and alleviate the shuttle effect of polysulfides at the interface, thus improving the electrochemical performance of lithium-sulfur batteries.

DFT calculations were applied to determine the adsorption and catalytic ability of the polysulfide in the presence of LaOCl. Fig. 2a and Fig. S5 (Supporting information) indicate that the optimized structure of Li_2S_6 and LaOCl exhibits a dual chemical interaction, which confirms the S atoms tending to bond with La atoms and the Li atoms preferring to bond with O atoms that reveal the bond lengths of 1.97 and 2.26 Å, respectively. The stronger bonding suggests that the transformation of polysulfides on the LaOCl surface is thermodynamically favorable. The adsorption energy of the LaOCl nanofiber matrix on the polysulfide is higher than that of the carbon matrix on the polysulfide compared to the carbon matrix [35], indicating that the LaOCl nanofiber matrix has a strong chemical affinity for the polysulfide (Fig. 2b). The sulfur conversion process on the LaOCl matrix is thermodynamically favorable (Fig. 2c), especially the final Li_2S_2/Li_2S conversion step as rate-determining step, which has lower Gibbs free energy barrier. These results demonstrate that LaOCl nanofibers play an important role in lowering the energy barrier and catalyzing the polysulfide conversion with a significant catalytic effect.

The cyclic voltammetry (CV) test was devoted to investigate the effect of LaOCl nanofibers on redox reaction process of sulfur electrode. As shown in Fig. 2d, the CV profiles of the lithium-sulfur batteries with LaOCl/S show significantly sharper and higher peaks compared to those of S, implying a faster polysulfides conversion. Furthermore, the peak at the LaOCl/S electrode shifts slightly to the right during the reduction reaction and significantly to the left

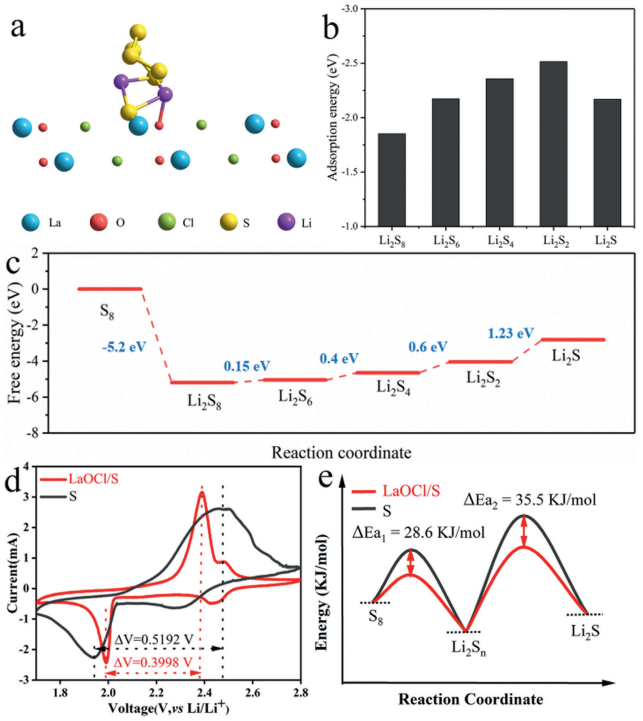

Fig. 2. (a) Optimized structure of Li_2S_6 on the surface of LaOCl nanofibers. (b) Adsorption energy of sulfur species on LaOCl nanofiber. (c) Gibbs free energy spectrum of sulfur transformation process on LaOCl nanofiber surface. (d) CV profiles of LaOCl/S and S cathodes at the scan rate of 0.1 mV/s. (e) E_a of the LaOCl/S and S cathodes in the discharge process.

during the oxidation reaction. Simultaneously, the LaOCl/S electrode exhibits the higher redox peak current and lower polarization demonstrating the improved redox reaction kinetics. The Tafel plots (Fig. S6 in Supporting information) for the oxidation and reduction processes were obtained from the CV curves, respectively. The Tafel equation ($\eta = a + b\log(i)$) was used to calculate corresponding exchange current densities [36]. It is calculated that the electrode with LaOCl/S has the higher exchange current density with 110 and 64 mA/cm^2 for the oxidation process and reduction process, respectively, compared to 267 and 128 mA/cm^2 for S electrode. For the reduction process from Li_2S_n to Li_2S, the Tafel slope at anodic sweep is 66 mV/dec for LaOCl/S electrode and 156 mV/dec for S electrode. For the transition from S_8 to long-chain Li_2S_n, the LaOCl/S electrode also has the smallest Tafel slope at the cathodic sweep. The lower Tafel slope reveals the better catalytic activity [37]. Therefore, LaOCl/S electrode exhibits the highest catalytic activity to accelerate the polysulfide conversion reactions.

Fig. 2e shows the result of activation energy gap between two electrodes using the equation ($E_{a,Red} = E^0{}_{a,\,Red} - RT/b\varphi_{cathode}$) based on the Tafel plots and CV curves [38,39]. The E_a values of both steps are remarkably reduced when the LaOCl nanofibers are added to S electrode, where the E_a differences between the LaOCl/S and pure sulfur electrode are 35.5 kJ/mol and 49.1 kJ/mol for the conversion reactions from S_8 to Li_2S_n (E_{a1}) and from Li_2S_n to Li_2S (E_{a2}), respectively. The smaller Ea means a beneficial effect of LaOCl nanofibers on redox kinetics. As can be seen from Fig. S7a, the two reduction peaks of the LaOCl/S electrode are positively shifted compared to that of the S electrode, while the oxidation peak is significantly negatively shifted, indicating that the electrocatalysis of LaOCl promotes the kinetics. Furthermore, the process of polysulphide redox can be studied by changing the redox onset potential, as shown in Fig. S7b (Supporting information). Compared to S, LaOCl/S increased the onset potential of the discharge peak and decreased the onset potential of the charge peak, indicating that the LaOCl can suppress the shuttle effect and promote the redox reaction of polysulfide. Meanwhile, the initial three cyclic voltammogram of LaOCl/S electrodes (Fig. S8 in Supporting information) show higher redox peak current and smaller redox potential gaps, which indicates the facilitated redox reactions in the LaOCl/S electrode. Furthermore, the CV curves overlap well in the initial three cycles and the positions of the reduction and oxidation peaks remained essentially unchanged, demonstrating the good electrochemical reversibility and stability of LaOCl/S electrode.

To further investigate the electrochemical performance of LaOCl nanofibers influencing on redox kinetics of sulfur cathode, the CV measurements were performed at various scanning rates. It is clearly observed from Fig. 3a and Fig. S9 (Supporting information) that the CV curves of the LaOCl/S and S electrodes shift towards higher potentials for the anodic peak and towards lower potentials for the cathodic peak as the scan rate increases. Based on the CV analysis at various scanning rates, the lithium-ion diffusion coefficient as kinetics descriptor can reflect conversion efficiency of sulfur species, which was quantitatively estimated according to the Randles-Sevcik equation [40,41]: $I_p = (2.69 \times 10^5) n^{3/2} A D_{Li^+}^{1/2} C_{Li^+} \nu^{1/2}$, where I_p is the peak current, n is the number of charge transfer electrons, A is the active surface area of the reacting electrode, D_{Li^+} is the lithium ions diffusion coefficient, C_{Li^+} is the lithium ions concentration, and ν is the scan rate. The lithium ions diffusion coefficient is only related to the square root of the peak current and scan rate. Figs. 3b and c show that the calculated slope of the S electrode is significantly smaller than that of the LaOCl/S electrode, while the consistent high slope of the oxidation and reduction peaks of the LaOCl/S electrode indicates its high catalytic activity and affinity for lithium polysulfide. The LaOCl/S electrode exhibits excellent lithium ions diffusion coefficients of 13.1 and 6.05×10^{-8} cm^2/s in both oxidation and reduction processes, which are superior to those of S electrode (3.25 and 2.54×10^{-8} cm^2/s). These results obviously demonstrate that the LaOCl/S electrode has higher polysulfide adsorption capacity compared with the S electrode, which can increase the conversion rate of polysulfide and improve the electrochemical reaction rate, resulting in a superior electrochemical performance.

The initial five charge/discharge curves at 0.1 C of the S and LaOCl/S electrodes are shown in Figs. 3d and e. Obviously, the charge/discharge potential plateaus are consistent with the anodic/cathodic peak potentials in cyclic voltammogram. Significantly, the lithium-sulfur batteries assembled with the LaOCl/S electrode show a promising initial specific capacity of 1112.3 mAh/g compared to the S electrode (1088.9 mAh/g). The corresponding differential capacity profile (Fig. S10 in Supporting information) displays two reduction peaks and oxidation peaks, which indicates the consistency of the voltage plateau in galvanostatic profiles. For the capacity contribution of sulfur cathode, LaOCl nanofibers are inactive and cannot provide capacity (Fig. S11 in Supporting information). The polarization overpotential of LaOCl/S (206 mV) is smaller than that of S (284 mV). The catalytic capacity of LaOCl nanofibers toward the sulfur species conversion can be quantified by the Q_L/Q_H ratio during cycles. Q_H and Q_L are the discharge capacity of the high and low voltage platform, respectively. The Q_L/Q_H ratio reflects the conversion capacity of the polysulfides [42]. Calculating the Q_H and Q_L values of LaOCl/S and S, the Q_L/Q_H ratio of LaOCl/S electrode approximates 3, which is higher than that of S electrode, indicating that polar LaOCl nanofibers can significantly improve the conversion of Li_2S_n to Li_2S_2/Li_2S. After five cycles, the typical voltage plateau of the LaOCl/S electrode overlaps better, demonstrating that the LaOCl/S electrode can suppress the shuttle effect and enhance the reversibility of the electrochemical reaction. These attractive results demonstrate that the porous

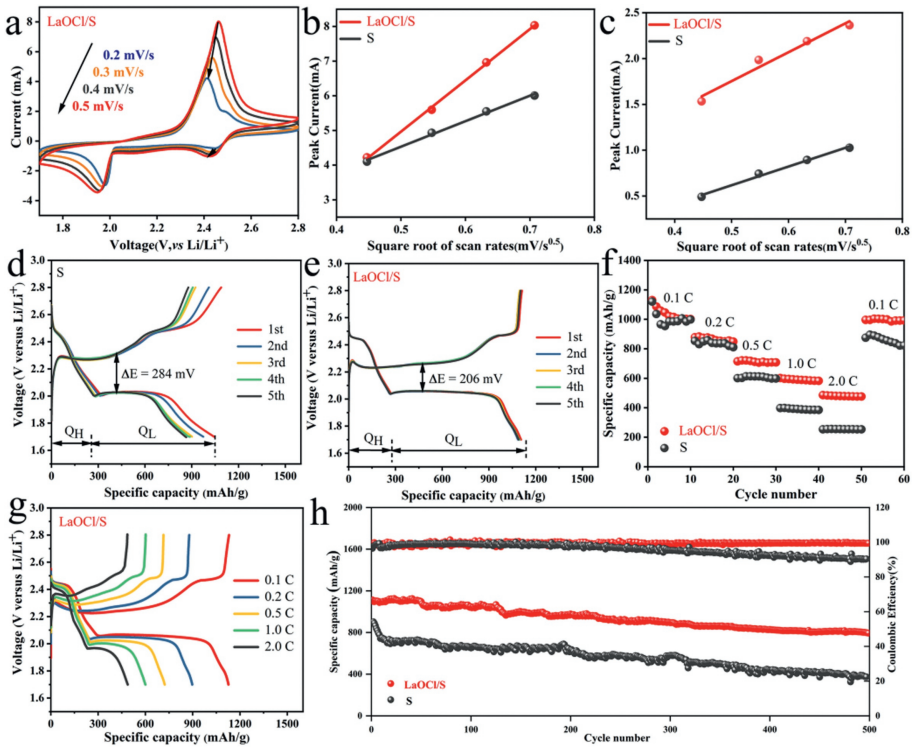

Fig. 3. (a) CV curves of LaOCl/S at different scan rates. CV peak current of (b) oxidation and (c) reduction process versus the square root of the scan rates. (d, e) Charge/discharge curves of different cycles at 0.1 C for S and LaOCl/S electrodes. (f) Rate behavior of different electrodes. (g) Galvanostatic discharge/charge profiles of LaOCl/S electrodes at current density varying from 0.1 C to 2 C. (h) cycling performance of S and LaOCl/S electrodes at 0.1 C.

LaOCl nanofibers have attractive chemisorption and catalytic activation, which are closely related to the cycling performance [43].

The rate performance of electrode materials is an important indicator for assessing the practicability of lithium-sulfur batteries. Fig. 3f shows the rate performance of LaOCl/S and S electrodes. The battery assembled with LaOCl/S electrode maintains specific discharge capacities of 1086.1, 882.6, 721.1, 601.3, and 485.5 mAh/g at various current densities of 0.1, 0.2, 0.5, 1.0, and 2.0 C, respectively. When returning to the rate of 0.1 C, a high discharge specific capacity of 1003.7 mAh/g can be still maintained, showing excellent reversibility and stability at various rates. However, an inferior rate capacity is exhibited for the S electrode, especially at high current rate of 2.0 C. The excellent electrochemical performance of LaOCl/S is attributable to the strong polar adsorption for polysulfide and the larger specific surface area of the porous LaOCl nanofibers. Fig. 3g shows the discharge/charge voltage distribution of LaOCl/S electrode at different current densities. The typical voltage plateaus of the LaOCl/S electrode can all be transferred slightly to the lower voltage side and remain stable at different current densities. In contrast, the S electrode exhibits a high polarization potential and the lack of discharge plateaus under high rate (Fig. S12 in Supporting information), which can be attributed to the serious potential barrier and the sluggish redox of the polysulfides. Compared with pristine sulfur electrode, LaOCl/S electrode reveals higher ratio of Q_L/Q_H at various current densities (Fig. S13 in Supporting information). The cycle performance of the LaOCl/S and S electrodes are indicated in Fig. 3h. The LaOCl/S cathode exhibit an average Coulombic efficiency of approximately 99.2% and a decay rate of 0.06% per cycle after 500 cycles. In contrast, the discharge capacity of S cathode rapidly decreases during 500 cycles. These results indicate that porous LaOCl nanofibers with abundant adsorption and catalytic sites can reasonably regulate polysulfide shuttling and facilitate the redox kinetics of sulfur species, thus effectively improving electrochemical performance [44]. In addition, the electrochemical impedance spectra (EIS) of the LaOCl/S and S electrodes before and after cycling be performed to ascertain the resistances (Fig. S14 in Supporting information). The EIS curves before cycling consist of a semicircle in the high frequency region and a straight line in the low frequency region, representing the charge transfer resistance (R_{ct}) and lithium ions diffusion impedance (W_0), respectively [45,46]. After 500 cycles, another semicircle is formed in the mid-frequency region due to the formation of Li_2S/Li_2S_2 on the electrode surface during charging and discharging. The electrolyte resistance R_s of the batteries with S electrode is relatively higher due to the dissolution of polysulfides. The R_{ct} of LaOCl/S electrode is lower than that of S electrode, indicating that LaOCl/S facilitates the polysulfides conversion and promotes the redox reaction. Furthermore, after the cycles of the LaOCl/S electrode, the separator is slightly colored with the polysulfides in comparison to the yellowish separators of the batteries with sulfur electrode (Fig. S15 in Supporting information). Raman spectra of the separator in the batteries with different cathodes after cycles further revealed that the characteristic signals intensity of the polysulfides weaken with the introduction of LaOCl, indicating effective inhibition of polysulfide shuttling (Fig. S16 in Supporting information). Thus, the unique porous LaOCl nanofibers as catalyst ensures the ion transport and conversion, which effectively inhibits the shuttle effect of polysulfides and regulate the reaction kinetics in lithium-sulfur batteries, thus exhibiting good electrochemical performance.

For commercial development of lithium-sulfur batteries, high sulfur loading is required to obtain high energy density system. Fig. 4a and Fig. S17 (Supporting information) show the electrochemical cycling performance under a high sulfur loading of 4.6 mg/cm^2. A reversible areal capacity of 4.2 mAh/cm^2 is delivered with an average Coulombic efficiency of approximately 98.6% and capacity retention of 83.4% after 150 cycles at 0.2 C. Fig. 4b shows the

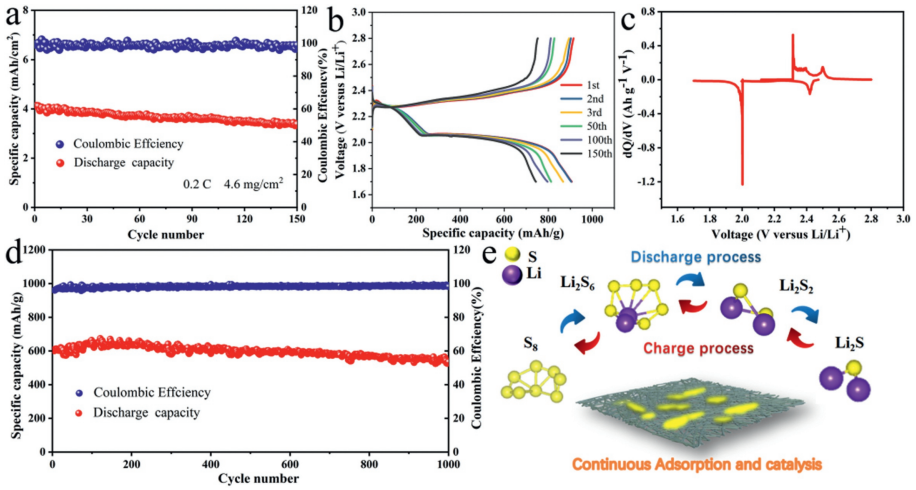

Fig. 4. (a) Areal capacity of LaOCl/S cathode at 0.2 C under 4.6 mg/cm^2 sulfur loading. (b) Charge/discharge curves of different cycles at 0.2 C. (c) Charge/discharge curve differential graphs. (d) Schematic of reaction mechanism of LaOCl nanofibers on polysulfides. (e) Long cycling performance of LaOCl/S electrodes at 1 C.

charge and discharge curves of LaOCl/S electrodes at 0.2 C under a high sulfur load of 4.6 mg/cm^2. After 150 cycles, two typical voltage plateaus can still be observed, which proves that LaOCl/S electrodes can suppress the shuttle effect and improve the electrochemical reversibility. The corresponding differential capacity profiles (Fig. 4c) display two reduction peaks and oxidation peaks, clearly illustrating the serial conversion reactions between active sulfur and Li_2S. To further demonstrate the lithium-sulfur batteries practicability, the long cycle performance of the batteries with porous LaOCl nanofibers was investigated at high currents of 1.0 C. In Fig. 4d, a high capacity of 565 mAh/g is maintained after 1000 cycles. Compared to the excellent sulfur-based electrodes that have been reported (Tables S1 and S2 in Supporting information), the LaOCl/S electrode has outstanding stability and reversibility. The excellent long cycle performance is attributed to porous LaOCl nanofibers with abundant adsorption and catalytic sites. The above results manifest the considerable advantages of porous LaOCl nanofibers as host for sulfur cathode. Benefitting from the porous architecture, LaOCl host provides sufficient load space and physical sulfur confinement (Fig. 4e). Simultaneously, polar LaOCl nanofibers can effectively inhibit the shuttle effect and promote reaction kinetics of sulfur species, thus obtaining the elevated capacity and prolonged the lifespan.

In summary, we synthesized a multifunctional host material with porous structure, adsorption and catalytic properties using electrostatic spinning and double crucible heating method. The shuttle effect of polysulfide is suppressed by increasing the redox reaction rate of polysulfide, which in turn promotes the electrochemical performance of lithium-sulfur batteries. Taking advantage of the above advantages, the prepared LaOCl/S electrodes exhibit a high initial discharge specific capacity of 1112.3 mAh/g at 0.1 C and remained a slight decay of 0.02% per cycle over 1000 cycles at 1.0 C. In addition, even at a high sulfur load of 4.6 mg/cm^2, the LaOCl/S cathode at 0.2 C still remained a high reversible areal capacity of 4.2 mAh/cm^2. The excellent electrochemical performance of the LaOCl/S cathode indicates that the rare earth chloride oxide nanomaterials have great potential to be used in lithium-sulfur batteries.

Declaration of competing interests

The authors declare that they have no known competing financial interests or personal relationships that could have appeared to influence the work reported in this paper.

Acknowledgments

This work was supported by the Scientific Research Program Funded by Education Department of Shaanxi Provincial Government (No. 22JK0411), the Natural Science Basic Research Program of Shaanxi Province (No. 2023-JC-QN-0165), and the National Natural Science Foundation of China (No. 21603109).

Supplementary materials

Supplementary material associated with this article can be found, in the online version, at doi:10.1016/j.cclet.2024.109691.

References

[1] Z.W. Seh, Y.M. Sun, Q.F. Zhang, Y. Cui, Chem. Soc. Rev. 45 (2016) 5605–5634.
[2] B. Scrosati, J. Hassoun, Y.K. Sun, Energy Environ. Sci. 4 (2011) 3287–3295.
[3] W.L. Qiu, G.R. Li, D. Luo, et al., Adv. Sci. 8 (2021) 2003400.
[4] Z. Zhang, J.N. Wang, A.H. Shao, et al., Sci. China Mater. 63 (2020) 2443–2455.
[5] P.P.R.M.L. Harks, C.B. Robledo, T.W. Verhallen, P.H.L. Notten, F.M. Mulder, Adv. Energy Mater. 7 (2017) 1601635.
[6] L. Jiao, C. Zhang, C.N. Geng, et al., Adv. Energy Mater. 9 (2019) 1900219.
[7] S.H. Chung, C.H. Chang, A. Manthiram, Adv. Funct. Mater. 28 (2018) 1801188.
[8] T.O. Ely, D. Kamzabek, D. Chakraborty, M. Doherty, ACS Appl. Energy Mater. 1 (2018) 1783–1814.
[9] Y. Zhao, Z. Gu, W. Weng, et al., Chin. Chem. Lett. 34 (2023) 107232.
[10] Y. Song, X. Li, C. He, Chin. Chem. Lett. 32 (2021) 1106–1110.
[11] J.Y. Li, J.X. Jiang, Y.G. Zhou, et al., Energy 285 (2023) 129434.
[12] X. Li, Y. Zhang, S. Wang, et al., Nano Lett 20 (2020) 701–708.
[13] A. Ghosh, M.S. Garapati, A.P.V.K. Saroja, R. Sundara, J. Phys. Chem. C 123 (2019) 10777–10787.
[14] L. Ma, B. Yue, X. Li, et al., Ceram. Int. 48 (2022) 22287–22296.
[15] T. Yi, L. Qiu, J. Mei, et al., Sci. Bull. 65 (2020) 546–556.
[16] J. Wu, Q.G. Feng, Y.C. Wang, et al., Chem. Commun. 59 (2023) 2966–2969.
[17] J.P. Mwizerwa, Q. Zhang, F.D. Han, et al., ACS Appl. Mater. Interfaces 12 (2020) 18519–18525.
[18] F. Li, L. Wang, G. Qu, et al., Chin. Chem. Lett. 33 (2022) 3909–3915.
[19] W.W. Sun, S.K. Liu, Y.J. Li, et al., Adv. Funct. Mater. 32 (2022) 2205471.
[20] Y. Yao, H.Y. Wang, H. Yang, et al., Adv. Mater. 32 (2020) 1905658.
[21] Z.H. Shen, Z.L. Zhang, M. Li, et al., ACS Nano 14 (2020) 6673–6682.
[22] M. Escudero-Escribano, P. Malacrida, M.H. Hansen, et al., Science 352 (2016) 73–76.
[23] T. Yi, L. Shi, X. Han, et al., Energy Environ. Mater. 4 (2021) 586–595.
[24] L. Peng, Z. Yu, M. Zhang, et al., Nanoscale 13 (2021) 16696–16704.
[25] J. Wu, T. Ye, Y.C. Wang, et al., ACS Nano 16 (2022) 15734–15759.
[26] H. Wang, X. Lai, C. Chen, et al., Chin. Chem. Lett. 34 (2023) 108473.
[27] Y. Tian, Y. Zhao, Y.G. Zhang, et al., ACS Appl. Mater. Interfaces 11 (26) (2019) 23271–23279.
[28] T. Wang, J.D. Chen, X.Y. Ren, et al., Angew. Chem. Int. Ed. 62 (2023) e202211174.
[29] Z.B. Zhao, H.N. Chang, R.Y. Wang, et al., Small Struct. 2 (2021) 2100069.
[30] C.Y. Wang, Y.J. Zhang, W.K. Wang, et al., Appl. Catal. B: Environ. 221 (2018) 320–328.
[31] G. Tekin, G. Ersoz, S. Atalay, J. Environ. Manage. 228 (2018) 441–450.

[32] Q.L. Bi, Q. Li, Z.P. Su, et al., Colloids Surf. A: Physicochem. Eng. Asp. 582 (2019) 123899.
[33] S. Wu, W.S. Yu, X.T. Dong, J.X. Wang, G.X. Liu, Chem. Eng. J. 266 (2015) 189–198.
[34] C.X. Zheng, D. Li, Q.L. Ma, et al., Chem. Eng. J. 310 (2017) 91–101.
[35] S. Yao, Y. Wang, Y. Liang, et al., Ceram. Int. 47 (2021) 27012–27021.
[36] C.J. Zhang, Y.P. He, Y.Q. Wang, et al., Appl. Surf. Sci. 560 (2021) 149908.
[37] X.Y. Yang, S. Chen, W.B. Gong, et al., Small 16 (2020) 2004950.
[38] Y.Q. Wang, H.L. Yu, A. Majeed, et al., J. Alloy. Compd. 891 (2022) 162074.
[39] Y.P. He, S.S. Yao, M.Z. Bi, et al., Electrochim. Acta 394 (2021) 139126.
[40] Y. Song, J. Wang, X. Li, et al., J. Colloid Interface Sci. 608 (2022) 963–972.
[41] Y.P. He, M.Z. Bi, H.L. Yu, et al., ChemElectroChem 8 (2021) 4564–4572.
[42] W.N. Ge, L. Wang, C.C. Li, et al., J. Mater. Chem. A 8 (2020) 6276–6282.
[43] K. Chang, W. Chen, Chem. Commun. 47 (2011) 4252–4254.
[44] R. Li, Z. Bai, W. Hou, et al., Chin. Chem. Lett. 34 (2023) 108263.
[45] X. Huang, C. Liu, Y. Lu, et al., J. Power Sources 382 (2018) 190–197.
[46] X. Dai, X. Wang, G. Lv, et al., Small 19 (2023) 2302267.